Higgs boson production at an electron-photon collider

N. Watanabe, Y. Kurihara[1]*, T. Uematsu*[2]*, K. Sasaki*[3]
1. High Energy Accelerator Research Organization (KEK), Tsukuba, Ibaraki 305-0801, Japan
2. Institute for Liberal Arts and Sciences, Kyoto University, Kyoto 606-8501, Japan
3. Faculty of Engineering, Yokohama National University, Yokohama 240-8501, Japan

Abstract
We investigate the Standard Model Higgs boson production in $e^-\gamma$ collisions. The electroweak one-loop contributions to the scattering amplitude for $e^-\gamma \to e^-H$ are calculated and expressed in analytical form. We analyze the cross section for the Higgs boson production in $e^-\gamma$ collisions for each combination of polarizations of the initial electron and photon beams. The feasibility of observing the Higgs boson in $e^- + \gamma \to e^- + b + \bar{b}$ channel is examined.

Keywords
Standard Model Higgs boson; $e^-\gamma$ collider; Backward Compton scattering.

1 Introduction

After a Higgs boson with mass 125 GeV was discovered by ATLAS and CMS at LHC [1], there has been growing interest in building a new accelerator facility [2], a linear e^+e^- collider, which offers much cleaner experimental collisions. Along with e^+e^- collider, other options such as e^-e^-, $e^-\gamma$ and $\gamma\gamma$ colliders have also been discussed [3, 4]. An e^-e^- collider is easier to build than an e^+e^- collider and may stand as a potential candidate before positron sources with high intensity are available. The $e^-\gamma$ and $\gamma\gamma$ options are based on e^-e^- collisions, where one or two of the electron beams are converted to the photon beams. In [5] we analyzed the Standard Model (SM) Higgs boson production in a e^- and real γ collision experiment,

$$e^-(k_1) + \gamma(k_2) \to e^-(k_1') + H(p_h)\ . \tag{1}$$

In this talk we summarize the results of [5].

2 Higgs boson production in $e^-\gamma$ collisions

The relevant Feynman diagrams for the process (1) start at the one-loop level in the electroweak interaction. We calculate the relevant one-loop diagrams in unitary gauge using dimensional regularization which respects electromagnetic gauge invariance. The one-loop diagrams which contribute to the reaction (1) are classified into four groups: $\gamma^*\gamma$ fusion diagrams (Fig. 1), $Z^*\gamma$ fusion diagrams, "$W\nu_e$" diagrams (Fig. 2) and "Ze" diagrams (Fig. 3).

Since k_2 is the momentum of a real photon, we have $k_2^2 = 0$ and $k_2^\beta \epsilon_\beta(k_2) = 0$, where $\epsilon_\beta(k_2)$ is the photon polarization vector. We set $q = k_1 - k_1'$. Assuming that electrons are massless so that $k_1^2 = {k_1'}^2 = 0$, we introduce the following Mandelstam variables: $s = (k_1 + k_2)^2$, $t = (k_1 - k_1')^2 = q^2$, $u = (k_1 - p_h)^2 = m_h^2 - s - t$, where $p_h^2 = m_h^2$ with m_h being the SM Higgs boson mass.

Charged fermions and W boson contribute to the one-loop $\gamma^*\gamma$ fusion diagrams. Since the couplings of the Higgs boson to fermions are proportional to the fermion masses, we only consider the top quark for the charged fermion loop diagrams. The $\gamma^*\gamma$ fusion diagrams we calculate are shown in Fig. 1. We obtain the contribution from the one-loop $\gamma^*\gamma$ fusion diagrams to the gauge-invariant scattering amplitude as follows:

$$A_{\gamma\gamma} = \left(\frac{e^3 g}{16\pi^2}\right)\left[\overline{u}(k_1')\gamma_\mu u(k_1)\right]\frac{1}{t}\left(g^{\mu\beta} - \frac{2k_2^\mu q^\beta}{m_h^2 - t}\right)\epsilon_\beta(k_2)\ F_{\gamma\gamma}\ , \tag{2}$$

https://doi.org/10.23727/CERN-Proceedings-2018-001.27

with

$$F_{\gamma\gamma} = \frac{2m_t^2}{m_W} N_c Q_t^2 \; S^{\gamma\gamma}_{(T)}(t, m_t^2, m_h^2) - m_W S^{\gamma\gamma}_{(W)}(t, m_W^2, m_h^2) \; , \tag{3}$$

where e, g, m_t and m_W are the electromagnetic and weak gauge couplings, the top-quark and W-boson masses, respectively, and $N_c = 3$ and $Q_t = \frac{2}{3}$. $S^{\gamma\gamma}_{(T)}$ and $S^{\gamma\gamma}_{(W)}$ are contributions from top loops and W loops, respectively, and are expressed in terms of the Passarino-Veltman two-point integrals B_0's and three-point integrals C_0's [6]. For their explicit expressions, see Eqs.(2.6) and (2.7) of Ref. [5]. Although the two-point integrals B_0's have ultraviolet divergences, these divergences are cancelled out when they are added and, therefore, $S^{\gamma\gamma}_{(T)}$ and $S^{\gamma\gamma}_{(W)}$ give finite results.

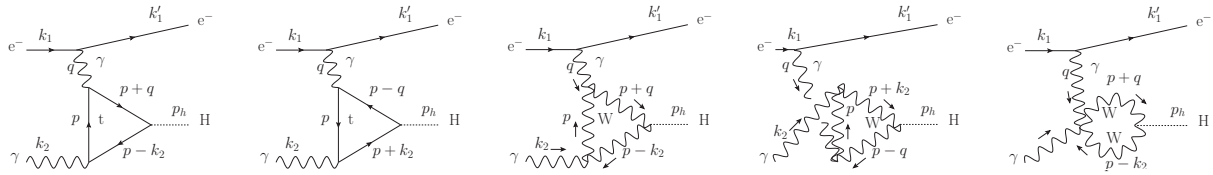

Fig. 1: $\gamma^*\gamma$ fusion diagrams: top-quark and W-boson loop contributions.

The one-loop $Z^*\gamma$ fusion diagrams for the Higgs boson production are obtained from the one-loop $\gamma^*\gamma$ fusion diagrams given in Fig. 1 by replacing the photon propagator with that of the Z boson with mass m_Z. Charged fermions and W boson contribute to the one-loop $Z^*\gamma$ fusion diagrams. Again we only consider the top quark for the charged fermion loop diagrams. We calculate the contribution from the $Z^*\gamma$ fusion diagrams and obtain,

$$A_{Z\gamma} = \left(\frac{eg^3}{16\pi^2}\right)\left[\overline{u}(k_1')\gamma_\mu\Big(f_{Ze} + \gamma_5\Big)u(k_1)\right]\frac{1}{t - m_Z^2}\Big(g^{\mu\beta} - \frac{2k_2^\mu q^\beta}{m_h^2 - t}\Big)\epsilon_\beta(k_2)\, F_{Z\gamma} \; , \tag{4}$$

with

$$F_{Z\gamma} = -\frac{m_t^2}{8m_W \cos^2\theta_W} N_c Q_t f_{Zt} S^{Z\gamma}_{(T)}(t, m_t^2, m_h^2) + \frac{m_W}{4} S^{Z\gamma}_{(W)}(t, m_W^2, m_h^2) \; , \tag{5}$$

where f_{Ze} and f_{Zt} are the strength of the vector part of the Z-boson coupling to the electron and top quark, respectively, and are given by $f_{Ze} = -1 + 4\sin^2\theta_W$ and $f_{Zt} = 1 - \frac{8}{3}\sin^2\theta_W$ with θ_W being the Weinberg angle. The axial-vector part of the Z-boson coupling to the top quark has a null effect and we find $S^{Z\gamma}_{(T)}(t, m_t^2, m_h^2) = S^{\gamma\gamma}_{(T)}(t, m_t^2, m_h^2)$ and $S^{Z\gamma}_{(W)}(t, m_W^2, m_h^2) = S^{\gamma\gamma}_{(W)}(t, m_W^2, m_h^2)$.

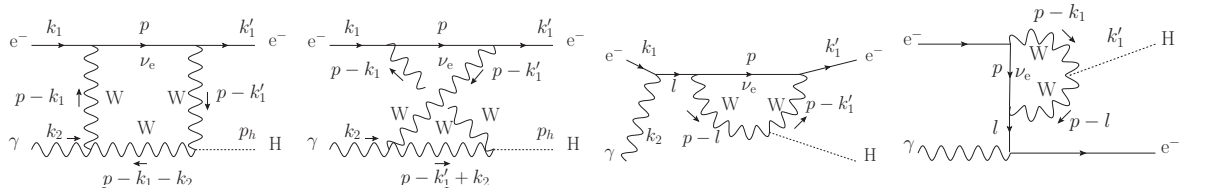

Fig. 2: "$W\nu_e$" diagrams.

The Feynman diagrams involving the W boson and electron neutrino, which are shown in Fig. 2, also contribute to the Higgs boson production in $e^-\gamma$ collisions. They yield the "$W\nu_e$" amplitude which is written in the following form,

$$A_{W\nu_e} = \left(\frac{eg^3}{16\pi^2}\right)\frac{m_W}{4}\left[\overline{u}(k_1')\; F_{(W\nu_e)\beta}\; (1 - \gamma_5)u(k_1)\right]\epsilon(k_2)^\beta \; , \tag{6}$$

where the factor $(1 - \gamma_5)$ is due to the e-ν-W vertex. Thus, when the electron beams are right-handedly polarized, these "$W\nu_e$" diagrams do not contribute. The factor $F_{(W\nu_e)\beta}$ is written in a gauge-invariant

form as

$$F_{(W\nu_e)\beta} = \left(\frac{2k_{1\beta}\not{k}_2}{s} - \gamma_\beta\right) S^{W\nu_e}_{(k_1)}(s,t,m_h^2,m_W^2) + \left(\frac{2k'_{1\beta}\not{k}_2}{u} + \gamma_\beta\right) S^{W\nu_e}_{(k'_1)}(s,t,m_h^2,m_W^2)\,, \tag{7}$$

where $S^{W\nu_e}_{(k_1)}$ and $S^{W\nu_e}_{(k'_1)}$ are expressed in terms of the scalar integrals B_0's, C_0's and the scalar four-point integrals D_0's. See Eqs.(2.15) and (2.16) of Ref. [5]. Again the ultraviolet divergences of B_0's cancel out and, in the end, $S^{W\nu_e}_{(k_1)}$ and $S^{W\nu_e}_{(k'_1)}$ are finite. Finally we note that $S^{W\nu_e}_{(k'_1)}$ vanishes at $u = 0$, which is anticipated from the expression of the second term in Eq. (7).

The last one-loop contributions to the Higgs boson production in $e^-\gamma$ collisions come from the Feynman diagrams shown in Fig. 3. These "Ze" diagrams give the following amplitude,

$$A_{Ze} = \left(\frac{eg^3}{16\pi^2}\right)\left(-\frac{m_Z}{16\cos^3\theta_W}\right) \times \left[\overline{u}(k'_1)\, F_{(Ze)\beta}\, (f_{Ze}+\gamma_5)^2 u(k_1)\right]\epsilon(k_2)^\beta\,, \tag{8}$$

where the factor $(f_{Ze}+\gamma_5)^2$ arises from the Z-boson coupling to electrons. The factor $F_{(Ze)\beta}$ is written in a gauge-invariant form as

$$F_{(Ze)\beta} = \left(\frac{2k_{1\beta}\not{k}_2}{s} - \gamma_\beta\right) S^{Ze}_{(k_1)}(s,t,m_h^2,m_Z^2) + \left(\frac{2k'_{1\beta}\not{k}_2}{u} + \gamma_\beta\right) S^{Ze}_{(k'_1)}(s,t,m_h^2,m_Z^2)\,, \tag{9}$$

where $S^{Ze}_{(k_1)}$ and $S^{Ze}_{(k'_1)}$ are expressed in terms of the scalar integrals B_0's, C_0's and D_0's. See Eqs.(2.19) and (2.20) of Ref. [5]. Collinear singularities appear in some of C_0's and D_0's. These collinear divergences are handled by dimensional regularization. Actually scalar integrals with collinear divergences appear in combination. When they are added their divergences cancel out. Thus $S^{Ze}_{(k_1)}$ and $S^{Ze}_{(k'_1)}$ are both finite. Note also that $S^{Ze}_{(k'_1)}$ vanishes at $u = 0$.

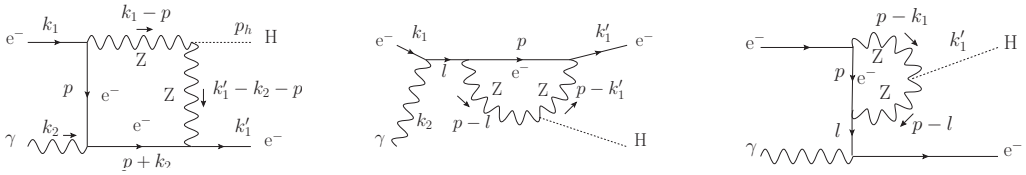

Fig. 3: "Ze" diagrams.

3 Numerical analysis

One of the advantages of linear colliders is that we can acquire highly polarized colliding beams. Let us consider the Higgs boson production reaction (1) when both the initial electron and photon beams are fully polarized. We denote the polarizations of the electron and photon as $P_e = \pm 1$ and $P_\gamma = \pm 1$, respectively. When an initial electron is polarized with polarization P_e, we modify $u(k_1)$ as $u(k_1) \to \frac{1+P_e\gamma_5}{2}\, u(k_1)$. And when a photon with momentum k_2 is moving in the $+z$ direction in the center-of-mass (CM) frame, the circular polarization ($P_\gamma = \pm 1$) of the photon is taken to be $\epsilon(k_2, \pm 1)_\beta = \frac{1}{\sqrt{2}}(0, \mp 1, -i, 0)$. Then the Higgs boson production cross section is given by

$$\sigma_{(e\gamma\to eH)}(s, P_e, P_\gamma) = \frac{1}{16\pi s^2}\int_{\rm cut} dt \left\{ \sum_{\text{final electron spin}} |A(P_e, P_\gamma)|^2 \right\}. \tag{10}$$

where $A(P_e, P_\gamma)$ is written at the one-loop level as

$$A(P_e, P_\gamma) = A_{\gamma\gamma}(P_e, P_\gamma) + A_{Z\gamma}(P_e, P_\gamma) + A_{W\nu_e}(P_e, P_\gamma) + A_{Ze}(P_e, P_\gamma)\,. \tag{11}$$

Since the forward and backward directions in an $e^-\gamma$ collider are blind spots for the detection of scattered particles, we introduce kinematical cuts for the scattered electron in $e^-\gamma$ collisions. Denoting θ as the angle between the initial and scattered electrons in the CM frame, we choose the allowed region of θ as $10^\circ \leq \theta \leq 170^\circ$, which leads to the integration range of t in Eq. (10) as $(-s + m_h^2 - t_{\rm cut}) \leq t \leq t_{\rm cut}$ with $t_{\rm cut} = -\frac{1}{2}(s - m_h^2)(1 - \cos 10^\circ)$. Note that $A_{W\nu_e} = 0$ when $P_e = +1$.

For numerical analysis we choose the mass parameters and the coupling constants as follows: $m_h = 125$ GeV, $m_t = 173$ GeV, $m_Z = 91$ GeV, $m_W = 80$ GeV, $\cos\theta_W = \frac{m_W}{m_Z}$, $e^2 = 4\pi\alpha_{em} = \frac{4\pi}{128}$ and $g = \frac{e}{\sin\theta_W}$. The electromagnetic constant e^2 is chosen to be the value at the scale of m_Z. We plot $\sigma_{(e\gamma\to eH)}(s, P_e, P_\gamma)$ in Fig. 4 as a function of $\sqrt{s}$ ($\sqrt{s} \geq 130$ GeV) for each case of polarizations of the electron and photon beams. For the case $P_eP_\gamma = -1$, the cross section $\sigma_{(e\gamma\to eH)}$ is very small at $\sqrt{s} = 130$ GeV, since the integration range of t is small and the differential cross section vanishes as $t \to t_{\rm min}$. The cross section $\sigma_{(e\gamma\to eH)}(s, P_e = -1, P_\gamma = +1)$ rises gradually up to about 2 fb, while $\sigma_{(e\gamma\to eH)}(s, P_e = +1, P_\gamma = -1)$ increases rather slowly up to 0.4 fb. This is due to the interference between $A_{\gamma\gamma}$ and $A_{Z\gamma}$, which acts constructively for $(P_e = -1, P_\gamma = +1)$ but destructively for $(P_e = +1, P_\gamma = -1)$. For the case $P_eP_\gamma = +1$, the cross section $\sigma_{(e\gamma\to eH)}$ is about 2 fb at $\sqrt{s} = 130$ GeV. The cross section $\sigma_{(e\gamma\to eH)}(s, P_e = -1, P_\gamma = -1)$ rises above 3 fb around $\sqrt{s} = 200$ GeV and then gradually decreases as $\sqrt{s}$ increases. This is due to the destructive interference both between $A_{W\nu_e}$ and $A_{\gamma\gamma}$ and between $A_{W\nu_e}$ and $A_{Z\gamma}$ in the range of large $-t$. Again the destructive interference between $A_{\gamma\gamma}$ and $A_{Z\gamma}$ is responsible for the decrease of $\sigma_{(e\gamma\to eH)}(s, P_e = +1, P_\gamma = +1)$ as $\sqrt{s}$ increases.

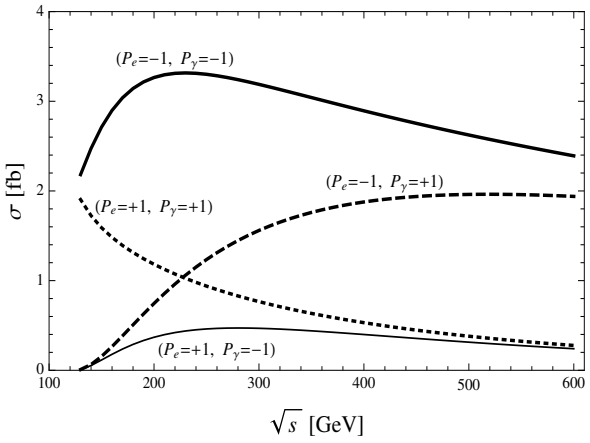

Fig. 4: Higgs boson production cross section $\sigma_{(e\gamma\to eH)}(s, P_e, P_\gamma)$. The kinematical cut is chosen such that the allowed angle θ of the scattered electron in the center-of-mass frame is $10^\circ \leq \theta \leq 170^\circ$.

A high-intensity photon beam can be produced by laser light backward scattering off a high-energy electron beam, $e^-\gamma_{\rm Laser} \to e^-\gamma$, where the backward-scattered photon receives a major fraction of the incoming electron energy [7]. Its energy distribution depends on the polarizations of the initial electron ($P_{e2} = \pm$) and laser photon ($P_{\rm Laser} = \pm$). Suppose we have a highly polarized e^-e^- collider machine. Converting one of the electron beams to photon beam by means of backward Compton scattering of a polarized laser beam, we obtain an $e^-\gamma$ collider with high polarization. The Higgs boson production cross section for $e^-\gamma \to e^-H$ in an e^-e^- collider, whose beam energies are E_{e1} and E_{e2} and polarizations are P_{e1} and P_{e2}, is expressed as,

$$\sigma_{e\gamma\ \text{collision}}(s_{ee}, E_{\rm Laser}, P_{e1}, P_{e2}, P_{\rm Laser}) = \sum_{P_\gamma} \int dy\ N(y, E_{e2}, E_{\rm Laser}, P_{e2}, P_{\rm Laser}, P_\gamma)\sigma_{(e\gamma\to eH)}(s, P_{e1}, P_\gamma), \tag{12}$$

where $\sigma_{(e\gamma\to eH)}(s, P_{e1}, P_\gamma)$ is given in Eq. (10) with P_e replaced by P_{e1}, and s_{ee} is the CM energy squared of the two initial electron beams and related to s as $s = ys_{ee}$. The photon energy is yE_{e2} and its spectrum is given by $N(y, E_{e2}, E_{\rm Laser}, P_{e2}, P_{\rm Laser}, P_\gamma)$ [8,9] with $P_{e2}P_{\rm Laser} = -1$. We take the case $P_{e2}P_{\rm Laser} = -1$ so that the spectrum has a peak at the highest energy.

We analyze the cross section of the Higgs boson production in an e^-e^- collider through $b\bar{b}$ decay channel, $e + \gamma \to e + H \to e + b + \bar{b}$, since it has a large branching ratio. We consider the case: $E_{\rm Laser} = 1.17$eV (the YAG laser with wavelength 1064nm) and E_{e2} =250GeV ($\sqrt{s_{ee}} = 500$GeV). The integration range of y in Eq. (12) is given by $y_{\rm min} \le y \le y_{\rm max}$ with $y_{\rm min} = 0.0625$ and $y_{\rm max} = 0.82$. The Monte Carlo method is used. A b-quark mass is chosen to be 4.3 GeV. The angle cuts of the scattered electron and $b(\bar{b})$ quarks are chosen such that the allowed regions are $10^\circ \le \theta_{e^-} \le 170^\circ$ and $10^\circ \le \theta_{b(\bar{b})} \le 170^\circ$, respectively, and the energy cuts of these particles are set to be 3GeV. The Monte Carlo statistical error is about 0.1% when sampling number is taken to be 200,000. The result is shown in Table 1 for each combination of polarizations P_{e1} and $P_{\rm Laser}$.

We also analyze the significance $S/\sqrt{B}$ of the Higgs boson production. The $b\bar{b}$ decay channel of the Higgs boson in $e^-\gamma$ collisions has a substantial background. Especially a huge background appears at the Z-boson pole. However, it is expected that when we measure the invariant mass $m_{b\bar{b}}$ of b and $\bar{b}$ quarks, the background is small in the region $m_{b\bar{b}}$ >120GeV compared with the signals of the Higgs boson production. We use GRACE [9] to write down all the tree Feynman diagrams for $e+\gamma \to e+b+\bar{b}$ and to evaluate their contributions to the background cross section. We assume that the integrated luminosity is 250fb^{-1}. The significance is calculated by taking samples in the region 120GeV $\le m_{b\bar{b}} \le$ 130GeV at the parton level. The results are given in Table 1. Large values of significance are obtained for the cases of $(P_{e1}, P_{\rm Laser}) = (-1, \mp 1)$ with $\sqrt{s_{ee}} = 500$GeV.

$\sqrt{s_{ee}}$ GeV	P_{e1}	$P_{\rm Laser}$	$\sigma_{\rm cut}$ fb	$S/\sqrt{B}$
500	1	-1	0.11	2.93
	1	1	0.19	1.31
	-1	-1	1.22	10.6
	-1	1	1.01	6.8

Table 1: Higgs boson production cross section and significance in $e^-\gamma$ collision in an e^-e^- collider for the case $E_{\rm Laser} = 1.17$eV, E_{e2} =250GeV, $\sqrt{s_{ee}}$ =500GeV, and for each combination of polarizations P_{e1} and $P_{\rm Laser}$. P_{e2} is chosen to be $-P_{\rm Laser}$.

4 Summary

We have investigated the SM Higgs boson production in $e^-\gamma$ collisions. The electroweak one-loop contributions to the scattering amplitude for $e^-\gamma \to e^-H$ were calculated and they were expressed in analytical form.ãĂĂ We analyzed the cross section of the Higgs boson production through the $b\bar{b}$ decay channel, $e + \gamma \to e + H \to e + b + \bar{b}$, in an $e^-\gamma$ collision in an e^-e^- collider. A high-energy photon beam was assumed to be produced by laser light backward scattering off one of the high-energy electron beams of the e^-e^- collider. We obtained large values of the significance $\sqrt{S}/B$ for the Higgs boson production for both $\sqrt{s_{ee}} = 250$GeV and $\sqrt{s_{ee}} = 500$GeV. We therefore conclude that the Higgs boson will be clearly observed in $e^-\gamma$ collision experiments.

Acknowledgements

We wish to thank the organizers of Photon 2017 for the hospitality at such a stimulating conference.

References

[1] ATLAS Collaboration, *Phys. Lett. B* **716** (2012) 1; CMS Collaboration, *Phys. Lett. B* **716** (2012) 30.

[2] http://www.linearcollider.org.

[3] A. De Roeck, arXiv:hep-ph/0311138 (2003); S. A. Bogacz *et al.*, arXiv:1208.2827 (2012); I. F. Ginzburg and M. Krawczyk, arXiv:1310.5881 (2013).

[4] V. I. Telnov, *Nucl. Instrum. Meth. A* **455** (2000) 63; B. Badelek *et al.*, *Int. J. Mod. Phys. A* **19** (2004) 5097; M. M. Velasco *et al.*, *eConf C* **010630** (2001) E3005.

[5] N. Watanabe, Y. Kurihara, T. Uematsu and K. Sasaki, *Phys. Rev. D* **90**, (2014) 033015.

[6] G. Passarino and M. Veltman, *Nucl. Phys. B* **160** (1979) 151.

[7] I. F. Ginzburg, G. L. Kotkin, V. G. Serbo, and V. I. Telnov, *Nucl. Instr. and Meth.* **205** (1983) 47.

[8] A. M. Sessler, *Conf. Proc. C* **950501** (1995) 30; K. Kim and A. Sessler, *SLAC Beam Line* **26** (1996) 16.

[9] F. Yuasa, Y. Kurihara and S. Kawabata, *Phys. Lett. B* **414** (1997) 178; F. Yuasa *et al.*, *Prog. Theor. Phys. Suppl.* **138** (2000) 18.